

Article

Three-Dimensional Hierarchical Hydrotalcite–Silica Sphere Composites as Catalysts for Baeyer–Villiger Oxidation Reactions Using Hydrogen Peroxide

Daniel Cosano *, Dolores Esquivel , Francisco J. Romero-Salguero , César Jiménez-Sanchidrián and José Rafael Ruiz * 

Departamento de Química Orgánica, Facultad de Ciencias, Campus de Rabanales, Instituto Universitario de Investigación en Química Fina y Nanoquímica IUNAN, Universidad de Córdoba, Edificio Marie Curie, 14071 Córdoba, Spain; q12esmem@uco.es (D.E.); qo2rosaf@uco.es (F.J.R.-S.); qo1jsac@uco.es (C.J.-S.)

* Correspondence: q92cohid@uco.es (D.C.); qo1ruarj@uco.es (J.R.R.);

Tel.: +34-957-218623 (D.C.); +34-957-218638 (J.R.R.)

Abstract: The development of effective, environmentally friendly catalysts for the Baeyer–Villiger reaction is becoming increasingly important in applied catalysis. In this work, we synthesized a 3D composite consisting of silica spheres coated with Mg/Al hydrotalcite with much better textural properties than its 2D counterparts. In fact, the 3D solid outperformed a 2D-layered hydrotalcite as catalyst in the Baeyer–Villiger reaction of cyclic ketones with H₂O₂/benzotrile as oxidant. The 3D catalyst provided excellent conversion and selectivity; it was also readily filtered off the reaction mixture. The proposed reaction mechanism, which involves adsorption of the reactants on the hydrotalcite surface, is consistent with the catalytic activity results.

Keywords: three-dimensional hierarchical materials; Baeyer–Villiger reaction; hydrogen peroxide; hydrotalcite; silica



Citation: Cosano, D.; Esquivel, D.; Romero-Salguero, F.J.; Jiménez-Sanchidrián, C.; Ruiz, J.R. Three-Dimensional Hierarchical Hydrotalcite–Silica Sphere Composites as Catalysts for Baeyer–Villiger Oxidation Reactions Using Hydrogen Peroxide. *Catalysts* **2022**, *12*, 629. <https://doi.org/10.3390/catal12060629>

Academic Editors: Lucjan Chmielarz and Roman Dziembaj

Received: 16 May 2022

Accepted: 7 June 2022

Published: 8 June 2022

Publisher's Note: MDPI stays neutral with regard to jurisdictional claims in published maps and institutional affiliations.



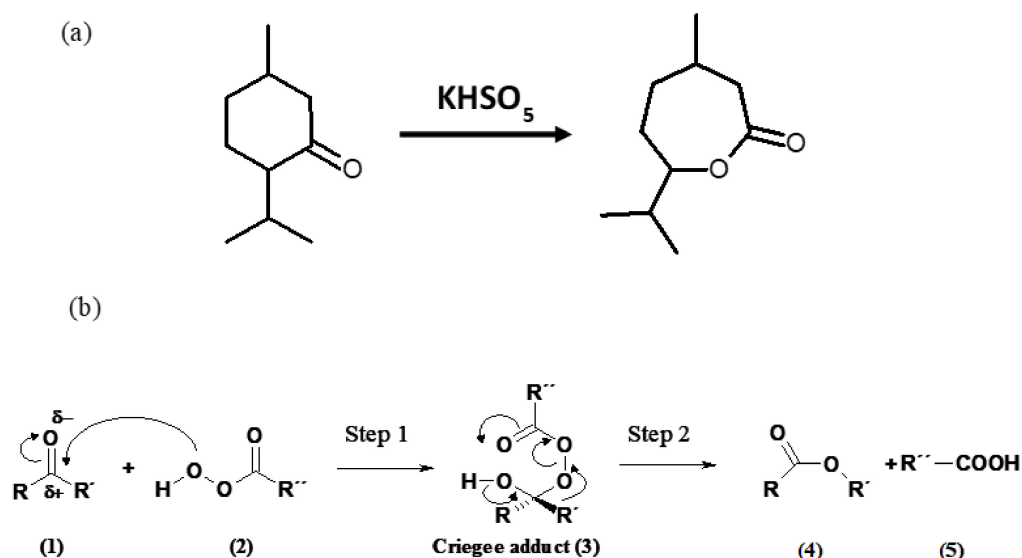
Copyright: © 2022 by the authors. Licensee MDPI, Basel, Switzerland. This article is an open access article distributed under the terms and conditions of the Creative Commons Attribution (CC BY) license (<https://creativecommons.org/licenses/by/4.0/>).

1. Introduction

One of the major aims of Green Chemistry is successfully combining the use of environmentally friendly reagents and heterogeneous catalysts [1] and one of the processes that has been successfully adapted to its requirements is the Baeyer–Villiger reaction, by which a ketone is oxidized to an ester with an organic peroxide. The original reaction developed by Baeyer and Villiger [2] involved treating menthone and carvomenthone with a mixture of potassium monopersulfate and sulfuric acid (see Scheme 1a). Since then, the reaction has been the subject of much research and conducted with a variety of reagents and catalysts [3–7]. The reaction takes place in two steps (Scheme 1b), the first involving a nucleophilic attack of the oxygen atom in the peracid on the carbonyl group of the ketone to form a Criegee adduct. In the second step, the adduct rearranges to the corresponding ester and a carboxylic acid is formed as a by-product. Hazardous reagents, which additionally lead to unwanted by-products, can be avoided by using hydrogen peroxide in the presence of a solid catalyst as oxidant. A variety of catalysts have been used for this purpose [6,7] including layered double hydroxides (LDHs), also known as hydrotalcite-like compounds or, simply, “hydrotalcites” (HTs) [8–12]. Our group has ample experience in the use of HTs [13–15] and structurally similar solids [16,17].

Hydrotalcites are a family of natural and synthetic products structurally consisting of brucite-like layers (viz., Mg(OH)₆ octahedra) and exchangeable anions in their interlayer region. Their general formula is M(II)_{1–x}M(III)_x[(OH)₂]^{x+}[X_{n/x}]^{n–}·mH₂O, where M(II) is a divalent metal, M(III) a trivalent metal and X the interlayer anion [18,19]. Replacing M(II) with M(III) in brucite-like layers produces a charge deficiency that is offset by interlayer anions, whether inorganic or organic [20]. So, a widely variable chemical composition also

results in variable physicochemical properties that have promoted extensive use HTs in a number of scientific fields [21–25].



Scheme 1. Baeyer-Villiger reaction (a) original reaction and (b) generally accepted mechanism [6].

Although hydrotalcites are easily prepared, the methods typically used to obtain them (*viz.*, coprecipitation and hydrothermal synthesis) produce poorly crystalline two-dimensional solids. Hydrotalcites used as catalysts in the Baeyer–Villiger reaction usually require a nitrile to combine with hydrogen peroxide on their surface to form a peroxy-carboximidic acid—the actual oxidant [13,14]. In this form, however, the catalytic process only occurs on the outer surface of the hydrotalcite. Therefore, improving HT activity entails increasing the active surface.

New synthetic methods have allowed hierarchical three-dimensional (3D) hydrotalcites to be developed for a number of uses such as nanotechnological applications [26–28]. The new family of materials includes hydrotalcite–silica composites [29–32]. Silica nanostructures consist of orderly frameworks [33] that allow the position of silicon atoms to be changed in order to obtain specific forms such as nanospheres, nanotubes or nanowires [34]. Silica has a nonporous surface with a 3D network of silanol (Si–OH) and siloxane (Si–O) groups. Silica particles aggregate through interaction between their silanol groups and create negative surface charge [35]; as a result, they can in theory be used as nucleation sites for HT growth. SiO₂@HT hierarchical structures are usually prepared layer-by-layer or by *in situ* growth [36]; the latter method involves coprecipitation from a suspension of structured silica. In previous work [37], our group reported the synthesis and structural characterization of silica microspheres coated with Mg/Al hydrotalcite layers. In this work, we used them as catalysts in the Baeyer–Villiger oxidation of cyclic ketones with hydrogen peroxide.

2. Results and Discussion

2.1. Characterization of Catalysts

Table 1 shows the mole ratios of the SiO₂@HT. As can be seen, the Mg/Al ratio was close to its theoretical value of 2, and so were the Si/Mg and Si/Al ratios to theirs. The table additionally shows the surface Mg/Al ratio as determined by XPS (entry 4). This ratio was lower than the total value, which is consistent with previous results of our group for hydrotalcites containing Mg and Al in variable proportions [38]. The elemental analysis and thermogravimetric results (Figure S5) were used to determine the formula of the resulting hydrotalcite, which was Mg_{0.657}Al_{0.343}(OH)₂(A)_{0.172}·0.58H₂O (where (A) is the interlaminal anion), and also that the catalysts consisted of 57.1 wt% hydrotalcite and 32.9 wt% SiO₂.

Table 1. Theoretical and experimental element ratios for the catalyst (SiO₂@HT) as determined by ICP-MS.

Entry	Molar Ratio	Theoretical	Experimental
1	Mg/Al	2.00	1.97
2	Si/Mg	0.83	0.85
3	Si/Al	1.67	1.67
4	Mg/Al ^a	-	1.46

^a Determined by XPS.

As noted earlier, similar solids were examined structurally in previous work. However, Figures S1–S4 show the results for the synthetic processes conducted here. As can be seen, the catalyst was successfully synthesized here as well.

SiO₂@HT was for the first time characterized in textural terms in this work. The specific surface area, cumulative pore volume and pore size distribution of a catalyst are highly influential on its activity. Nitrogen adsorption–desorption measurements were made in two solids. Figure 1a shows the resulting isotherm and the textural parameters derived from it. The surface area of SiO₂@HT was much higher than that of 2D layered hydrotalcites (Figure S5), which is typically around 70 m²/g; also, it clearly exceeded that of silica microspheres (ca. 20 m²/g). The isotherm was type IV in IUPAC's classification [39] and exhibited a well-defined hysteresis cycle over the range $0.4 < P/P_0 < 1$, suggesting the presence of mesopores. This was confirmed by the average pore diameter (ca. 10 nm) and the fact that it spanned a narrow range (i.e., that the pore size distribution was rather uniform). Furthermore, the hysteresis cycle was H2 type [39]. This is usually the case with porous sorbents such as inorganic oxide gels and porous glasses, which, however, have a more poorly defined pore size and shape. In fact, H2 cycles are especially difficult to interpret. Until a few decades ago, they were ascribed to a difference in mechanism between condensation and evaporation in pores with wide bodies but thin necks—often referred to as “ink-bottle pores”; at present, however, this is regarded as an oversimplified interpretation that ignores lattice effects.

2.2. Baeyer–Villiger Reaction

2.2.1. Kinetics of the Process

The Baeyer–Villiger reaction studied here was the oxidation of cyclohexanone to ϵ -caprolactone with hydrogen peroxide and benzonitrile at different temperatures. The optimum working conditions were established by following a kinetic procedure involving plotting the natural logarithm of the lactone concentration as a function of time. The plot was a straight line, which suggests first-order kinetics in the cyclohexanone concentration obeying the following law:

$$\ln (c_0/c) = k \cdot t, \quad (1)$$

where c_0 and c are the cyclohexanone concentrations at times zero and t , respectively; k is the rate constant and t time. A plot of $\ln (c_0/c)$ versus t thus gave the rate constant.

The influence of temperature on the reaction was examined over the range 40–90 °C. The results are shown in Table 2, entries 1–4, and the corresponding Arrhenius plot in Figure 2. As can be seen from the figure, a straight line was obtained, the slope of which allowed an activation energy of 19.40 kcal/mol to be calculated. Based on these results, we chose 90 °C as the optimum reaction temperature.

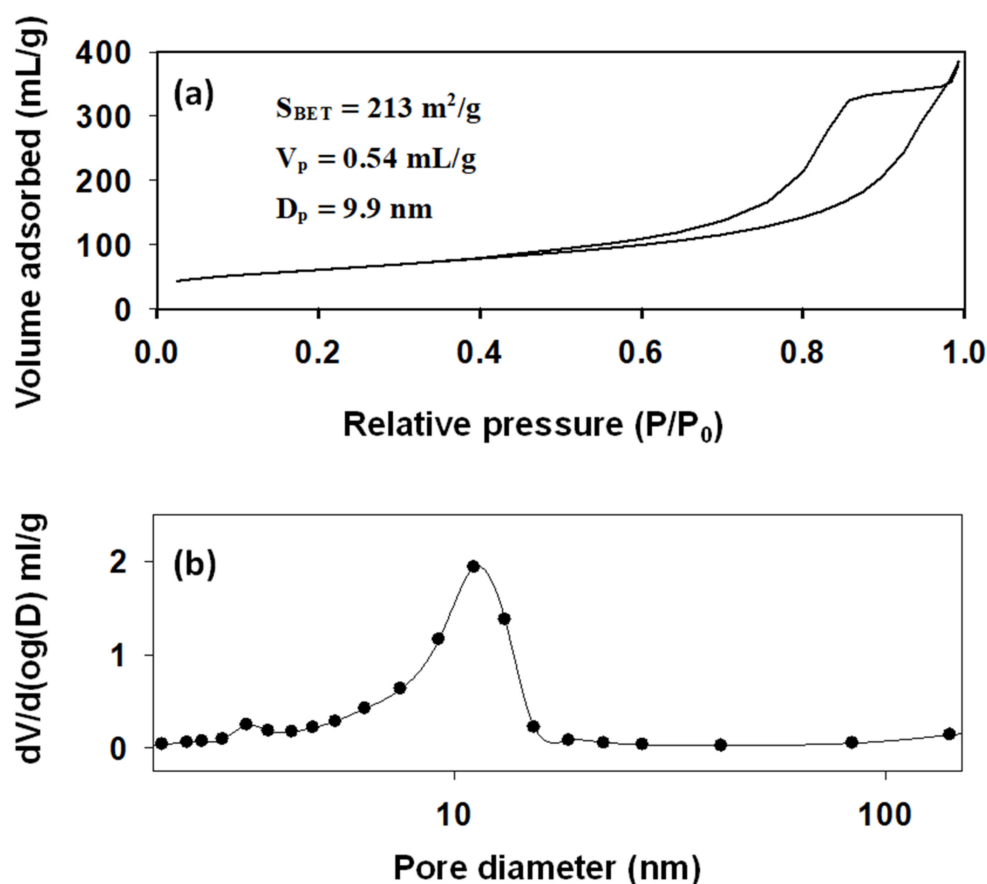
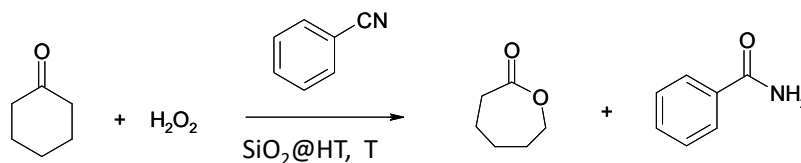


Figure 1. Nitrogen adsorption–desorption isotherm (a) and pore size distribution function (b) for the catalyst (SiO₂@HT). S_{BET} specific surface area; V_p cumulative pore volume; D_p average pore diameter.

Table 2. Influence of temperature on the Baeyer–Villiger oxidation of cyclohexanone with hydrogen peroxide ^a.



Entry	T (°C)	Conversion (%) ^b	$k \text{ (min}^{-1} \cdot \text{g}_{\text{cat}}) \cdot 10^{-4} \text{ }^c$
1	90	78	12.6
2	70	55	7.7
3	55	36	5
4	40	22	2.7
5 ^d	90	30	1.9
6 ^e	90	0	0
7 ^f	90	28	1.7
8 ^g	90	39	3.1

^a Reaction conditions: catalyst: 0.1 g; cyclohexanone = 6 mmol; hydrogen peroxide = 49 mmol; benzonitrile = 50 mmol; catalyst: 100 mg. ^b Conversion to ε-caprolactone (6 h); ^c rate constant; ^d reaction without catalyst; ^e reaction without nitrile; ^f reaction using SP-SiO₂ as catalyst; ^g reaction using layered HT-2D as catalyst.

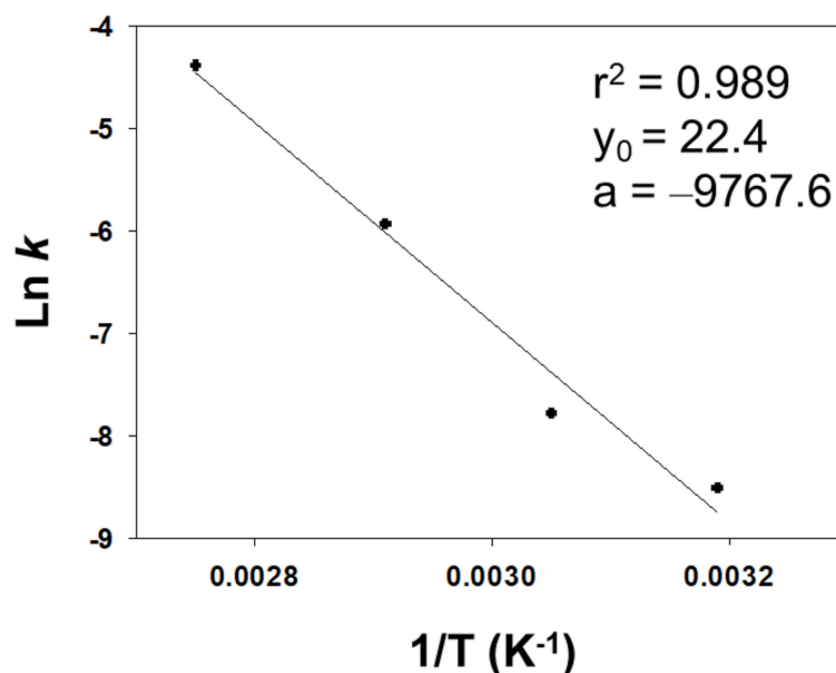


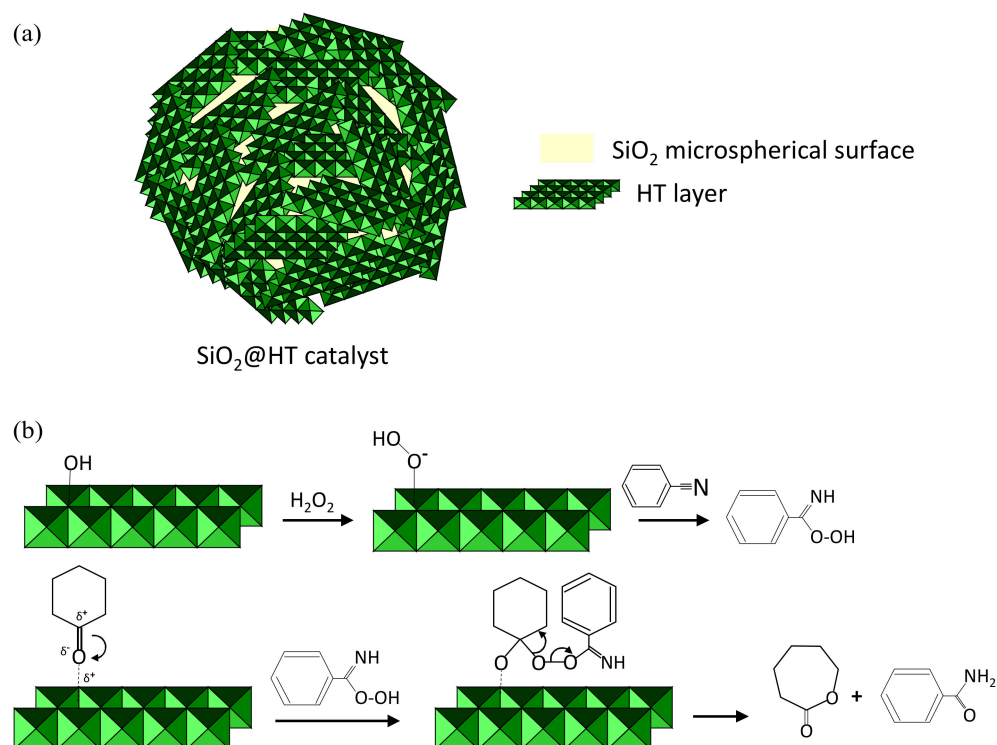
Figure 2. Arrhenius plot for the Baeyer–Villiger reaction of cyclohexanone on SiO₂@HT.

This determination was followed by blank tests intended to confirm that the reaction developed to no appreciable extent in the absence of catalyst and also that a nitrile was absolutely necessary for it to occur. The reaction also failed to develop (entries 5–7 in Table 2) in the absence of catalyst or nitrile, or in the presence of uncoated silica (SP-SiO₂). Therefore, the catalyst was indispensable. Finally, the catalyst (SiO₂@HT) was confirmed to be more active than a conventional 2D hydrotalcite by using one with an Mg/Al ratio of 2 similar to those used in previous studies [13–15]. Based on the results (Table 2, entry 8), the rate constant was four times higher with the 3D catalyst than with the 2D hydrotalcite.

To evaluate the catalytic performance of the 3D catalyst, comparisons with different materials were also made and the results are shown in Table S1. It was found that the catalyst had comparable or even better performance, indicating that it has a good catalytic performance.

2.2.2. Reaction Mechanism

The Baeyer–Villiger reaction of a cyclic ketone with a nitrile on a catalyst consisting of hydrotalcite-coated silica microspheres should take place through a mechanism similar to that observed with 2D layered hydrotalcites [13] (i.e., on the surface of the catalyst as shown in Scheme 2). Thus, the SiO₂@HT catalyst initially adsorbs hydrogen peroxide at surface basic sites to form an unstable hydroperoxide species that attacks nitrile molecules to form a peroxy-carboximidic acid—the actual oxidant. Then, the nucleophilic oxygen in the carbonyl group of the ketone is adsorbed on an electrophilic metal site of the catalyst for attack by the acid to form a Criegee-like adduct similar to those forming in homogeneous catalysis processes. Finally, the adduct rearranges to the lactone. Therefore, the improving textural properties of 3D hydrotalcite involved an increase of Brønsted basic centers (surface hydroxyl groups), which favor the formation of unstable hydroperoxide species [8,9,40–43].

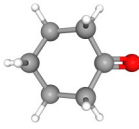
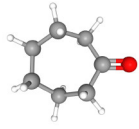
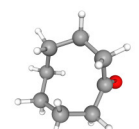
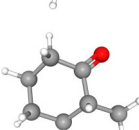
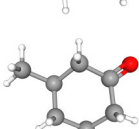
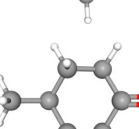
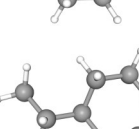
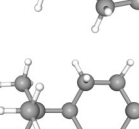


Scheme 2. Reaction of Baeyer–Villiger catalyzed by SiO₂@HT (a) Catalyst structure. (b) Mechanism for the Baeyer–Villiger reaction of cyclohexanone with benzonitrile and hydrogen peroxide on an HT layer in the catalyst.

2.2.3. Baeyer–Villiger Oxidation of Cyclic Lactones

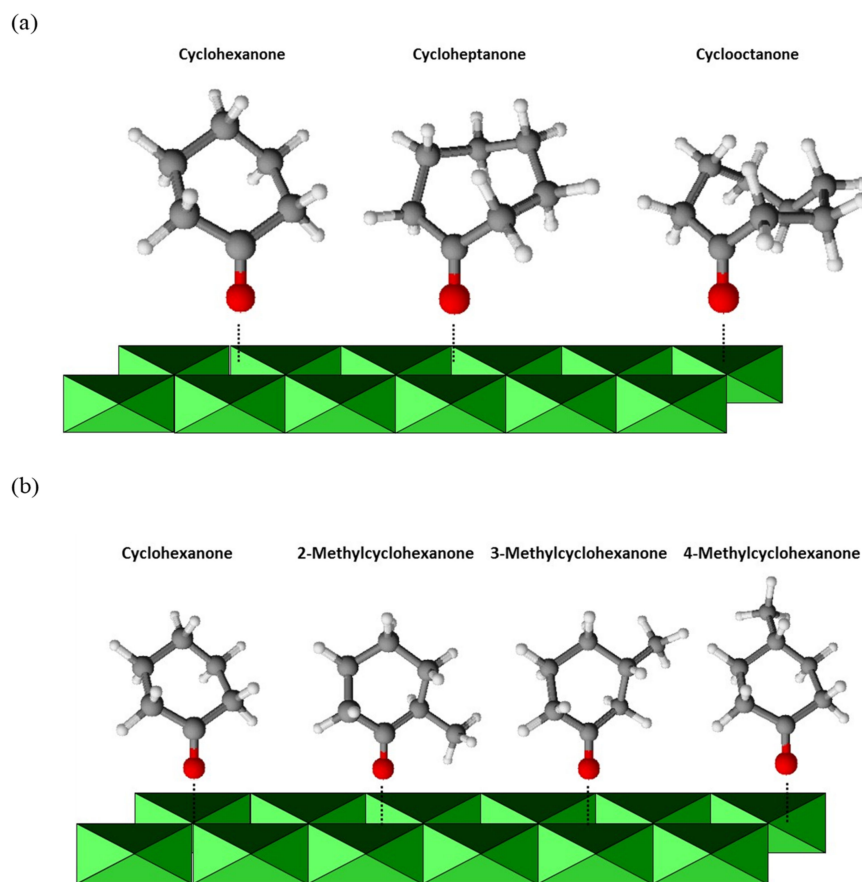
Once the optimum working conditions were established, the reaction was extended to other cyclic ketones (Table 3). Most were converted to their lactones with high selectivity and conversion. Ring size was very strongly influential on conversion and reaction rate. If only the ketone adsorption step is considered, then there should be little difference between the lactones with five to seven rings (Scheme 3a). By contrast, adsorption of cyclooctanone should be more markedly hindered and its reaction slower as a result—which was indeed the case, judging from entry 4 in Table 3. In addition, the reaction rate decreased with increasing ring size from five to seven carbon atoms (Table 3, entries 1–3). Based on adsorption provisions alone, the differences should not be too large, however. Therefore, they must depend on the ease with which a five-membered ring can be expanded to a six-membered ring (e.g., from cyclopentanone to cyclohexanone). Cyclohexanone is less easily expanded to a seven-membered lactone ring, so its reaction rate should also be lower. This is especially so with cycloheptanone. In fact, the seven-membered ring was difficult to cleave and reacted at a lower rate. Expanding cyclooctanone to a nine-membered ring is even more difficult, which, together with its more sterically hindered adsorption, led to its reaction being much slower than with the previous ketones.

Table 3. Structure, conversion, rate constant and selectivity in selected Baeyer–Villiger reactions.

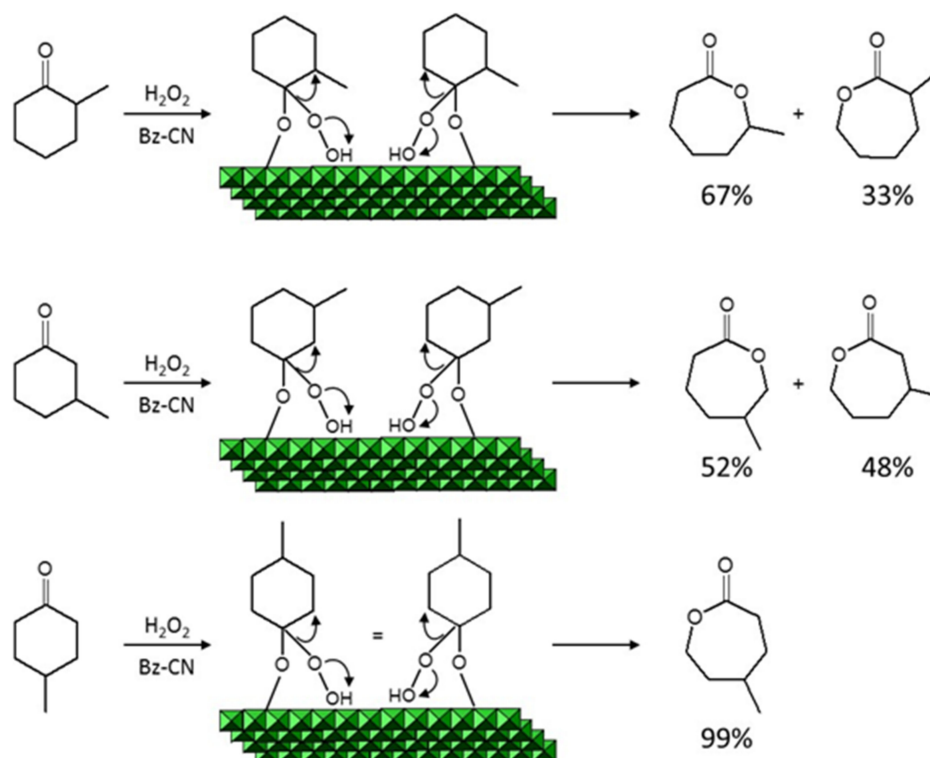
Entry	Name	Pubchem I.D.	Formule	φ (%) ^a	k (10^{-3}) (min^{-1}) ^b	S (%) ^c
1	Cyclohexanone	108-94-1		78	12.6	100
2	Cycloheptanone	502-42-1		50	8.3	100
3	Cyclooctanone	502-49-8		42	3.1	99
4	2-Methylcyclohexanone	583-60-8		59	9.9	67
5	3-Methylcyclohexanone	591-24-2		60	10.8	52
6	4-Methylcyclohexanone	589-92-4		78	12.3	99
7	4-Ethylcyclohexanone	5441-51-0		54	8.7	100
8	2-terc-butylcyclohexanone	98-53-3		52	6.4	100

^a Conversion to lactone (6 h); ^b rate constant; ^c selectivity to lactone (6 h).

The influence of the ease of ketone adsorption onto the catalyst on the reaction rate was examined by using cyclohexanones bearing a methyl substituent at position 2, 3 or 4 (Scheme 3b; Table 3, entries 5–7). The substituent at 2 strongly hindered adsorption of the substrate and considerably reduced the reaction rate as a result. Steric hindrance was less marked with the substituent at 3, so the reaction rate was higher than with 2-methylcyclohexanone. Finally, there was virtually no steric hindrance from the substituent at position 4 and the resulting reaction rate was similar to that with cyclohexanone. A bulkier substituent again reduced the reaction rate by hindering adsorption of the cyclohexanone ring. Furthermore, 2- and 3-methylcyclohexanone have an asymmetric structure that can lead to two different products (see Scheme 4), thereby detracting from selectivity. In addition, the reaction rate of cyclohexanones bearing a substituent is more markedly influenced by their ease of ring expansion than by that of adsorption. This is immediately apparent if one compares the conversion and rate values for cycloheptanone and cyclooctanone (entries 3 and 4 in Table 3 with those for 2-methylcyclohexanone (entry 5), for example.



Scheme 3. Structure of the cyclic ketones studied. (a) Difference between the cyclic ketones with five to seven rings (b) Difference between the cyclohexanones bearing a methyl substituent at position 2, 3 or 4.



Scheme 4. Intermediate adducts in the Baeyer–Villiger reaction of 2-, 3- and 4-methylcyclohexanone.

This section may be divided by subheadings. It should provide a concise and precise description of the experimental results, their interpretation, as well as the experimental conclusions that can be drawn.

3. Materials and Methods

3.1. Materials

3.1.1. Silica Microspheres

Silica microspheres were obtained according to Stöber [44]. A volume of 3.7 mL of tetraethyl orthosilicate (TEOS) was added to a solution containing 88 mL of ethanol and 12 mL of ammonia, the mixture being vigorously stirred at room temperature for 24 h. Then, the solid formed (SP-SiO₂) was isolated by centrifugation, washed with 300 mL of ethanol and dried in a stove at 70 °C overnight.

3.1.2. Hydrotalcite-Coated Microspheres

Three-dimensional materials were obtained as described elsewhere [37]. A volume of 200 mL of an aqueous solution containing 10 mmol of Mg(NO₃)₂·6H₂O and 5 mmol of Al(NO₃)₃·9H₂O was added to 500 mL of an also aqueous suspension containing 0.5 g of silica microspheres that was previously sonicated for 90 min to facilitate dispersion. The addition time was 2 h and pH 9, kept constant by adding 1 M NaOH as required. Then, the composite formed (SiO₂@HT) was filtered off and washed with bidistilled, de-ionized water.

3.1.3. Two-Dimensional Hydrotalcite

The 2D hydrotalcite used was prepared from solutions of Mg(NO₃)₂·6H₂O and Al(NO₃)₃·9H₂O in Mg (II)/Al(III) ratio of 2, using a coprecipitation method described elsewhere (ref). Typically, the mixture was slowly dropped over 500 mL of a solution of NaOH at pH 9 at 60 °C under vigorous stirring. Then, the material formed (HT-2D) was filtered off and washed with bidistilled, de-ionized water.

3.2. Characterization

The solids used were previously characterized in structural terms elsewhere [37]. However, the fact that the silica spheres were coated by hydrotalcite layers was confirmed with new analyses here. The results are shown in Figures S1–S4, Supplementary Materials. Those analyses were supplemented with others of texture including the determination of the Mg/Al, Si/Mg and Si/Al ratios by inductively coupled plasma mass spectrometry (ICP-MS). Samples were prepared on DigiPrep equipment, using Teflon vessels and a nitric acid medium at a programmed temperature for 90 min. The digestates thus obtained were diluted in 10% nitric acid for ICP-MS measurement. Elemental analyses were performed on a Perkin–Elmer NexION 350X ICP-MS instrument. Surface metal ratios were determined with a SPECS Phoibos HAS 3500 150 MCD X-ray photoelectron spectrometer (XPS) using a monochromatic Al anode (1486.7 eV). Accurate binding energies were determined relative to the position of Si 2p at 103.4 eV. Finally, moisture contents were determined by thermogravimetric analysis (TGA) on a Mettler Toledo balance. An air stream at 100 mL min^{−1} and a heating rate of 10 °C min^{−1} were used. The catalysts were characterized for texture by nitrogen adsorption–desorption porosimetry. Specific surface areas and pore size distributions were established with the Brunauer–Emmett–Teller (BET) and Barrett–Joyner–Halenda (BJH) methods, respectively. Nitrogen adsorption–desorption isotherms at −196 °C were obtained with an Autosorb-iQ MP/MP-XR instrument. All samples were outgassed at 60 °C overnight prior to measurement.

3.3. Reaction

Baeyer–Villiger reaction runs were performed at different temperatures in a two-neck flask containing 0.006 mol of cyclohexanone, 0.049 mol of nitrile, 0.05 mol of hydrogen peroxide and 0.1 g of catalyst. One of the neck's mouths was fitted with a reflux condenser

and the other was used for sampling at regular intervals. The reaction mixture was stirred throughout. Identical conditions were used in the reactions of the other cyclic ketones. Reaction products were identified from their retention times as measured with a Varian gas chromatograph equipped with a capillary column (VF-1MS, 15 m × 0.25 mm ID) and a flame ionization detector (FID).

4. Conclusions

A spherical hydrotalcite was obtained by coating silica microspheres with a layered double hydroxide. The resulting hierarchical 3D solid proved an excellent catalyst for the Baeyer–Villiger reaction of cyclic ketones with hydrogen peroxide and benzonitrile, which developed at a much higher rate than with a 2D hydrotalcite catalyst. As shown by the results, the reaction is strongly influenced by the adsorption of the ketone on the catalyst and the ease with which the ketone can undergo ring expansion. Thus, cyclopentanone exhibited the highest reaction rate because its adsorption was not being sterically hindered and its expansion to a six-membered lactone ring was quite easy. The reaction rate decreased with increasing ring size due to the increasing steric hindrance and decreasing ring expansion ability. The effect of steric hindrance was also apparent in cyclohexanones bearing a methyl substituent at position 2 or 3.

Supplementary Materials: The following supporting information can be downloaded at: <https://www.mdpi.com/article/10.3390/catal12060629/s1>, Figure S1: TG profiles for SiO₂@HT (solid line) and SP-SiO₂ (dashed line). Figure S2: XRD patterns for synthesized solids: HT-2D (a); SiO₂ microspheres; (b) and SiO₂@HT (c). Figure S3: μ -Raman spectra for synthesized solids: HT-2D (a); SiO₂ microspheres (b) and SiO₂@HT (c). Figure S4: TEM images for synthesized solids: (a) HT-2D; (b) SiO₂ microspheres and (c) SiO₂@HT. Figure S5: Nitrogen adsorption–desorption isotherm for (a) HT-2D and (b) SP-SiO₂. Table S1: Comparison of the prepared catalysts with those reported recently [17,28,44–52].

Author Contributions: D.C. and J.R.R. carried out the research sampling and processing. D.C. and J.R.R. performed the data analysis and interpretation. Critical review of the manuscript was realised by D.E., F.J.R.-S. and C.J.-S. All authors have read and agreed to the published version of the manuscript.

Funding: This research was funded by Spanish Ministry of Education and Science (Project RTI2018-101611-B-100).

Data Availability Statement: The authors declare that the manuscript is original and has not been submitted or published in any other journal, and the data in the manuscript is real.

Acknowledgments: The authors gratefully acknowledge funding by the Spanish Ministry of Education and Science (Project RTI2018-101611-B-100), D.C. acknowledges to 2014–2020 Social European Fund program of Andalusia (DOC_01376, FEDER).

Conflicts of Interest: The authors declare no conflict of interest.

References

1. Anastas, P.T.; Williamson, T.C. *Green Chemistry: An Overview*; ACS: Washington, DC, USA, 1996.
2. Baeyer, A.; Villiger, V. Einwirkung des caro'schen reagens auf ketone. *Berichte Der Deutschen Chemischen Gesellschaft* **1899**, *32*, 3625–3633. [[CrossRef](#)]
3. Krow, G.R. *The Baeyer-Villiger Reaction. Comprehensive Organic Synthesis*; Trost, B.M., Fleming, I., Eds.; Pergamon Press: Oxford, UK, 1991; Volume 7.
4. Strukul, G. Transition metal catalysis in the Baeyer–Villiger oxidation of ketones. *Angewandte Chemie Int. Ed.* **1998**, *37*, 1198–1209. [[CrossRef](#)]
5. Renz, M.; Meunier, B. 100 Years of Baeyer-Villiger Oxidations. *Eur. J. Org. Chem.* **1999**, *1999*, 737–750. [[CrossRef](#)]
6. Jiménez-Sanchidrián, C.; Ruiz, J.R. The Baeyer–Villiger reaction on heterogeneous catalysts. *Tetrahedron* **2008**, *9*, 2011–2026. [[CrossRef](#)]
7. Yan, F.; Li, C.; Liang, X.; Guo, S.; Fu, Y.; Chen, L. Baeyer-Villiger Reaction in Different Catalysis. *Recent Pat. Chem. Eng.* **2013**, *6*, 43–56. [[CrossRef](#)]
8. Kaneda, K.; Ueno, S. Development of hydrotalcite catalysts in heterogeneous Baeyer–Villiger oxidation. In *Heterogeneous Hydrocarbon Oxidation*; ACS Publications: Washington, DC, USA, 1996; ISBN 1947-5918.

9. Ueno, S.; Ebitani, K.; Ookubo, A.; Kaneda, K. The active sites in the heterogeneous Baeyer-Villiger oxidation of cyclopentanone by hydrotalcite catalysts. *Appl. Surf. Sci.* **1997**, *122*, 366–371. [[CrossRef](#)]
10. Pillai, U.R.; Sahle-demessie, E. Sn-exchanged hydrotalcites as catalysts for clean and selective Baeyer-Villiger oxidation of ketones using hydrogen peroxide. *J. Mol. Catal. A Chem.* **2003**, *191*, 93–100. [[CrossRef](#)]
11. Olszówka, J.; Karcz, R.; Napruszewska, B.D.; Duraczy, D.; Gawe, A.; Bahranowski, K.; Serwicka, E.M. Baeyer-Villiger oxidation of cyclohexanone with H₂O₂/acetonitrile over hydrotalcite-like catalysts: Effect of Mg/Al ratio on the ϵ -caprolactone yield. *Catal. Commun.* **2017**, *100*, 196–201. [[CrossRef](#)]
12. Karcz, R.; Olszówka, J.E.; Napruszewska, B.D.; Kry, J.; Serwicka, E.M.; Klimek, A.; Bahranowski, K. Combined H₂O₂/nitrile/bicarbonate system for catalytic Baeyer-Villiger oxidation of cyclohexanone to ϵ -caprolactone over Mg e Al hydrotalcite catalysts. *Catal. Commun.* **2019**, *132*, 4–8. [[CrossRef](#)]
13. Jimenez-Sanchidrian, C.; Hidalgo, J.M.; Llamas, R.; Ruiz, J.R. Baeyer-Villiger oxidation of cyclohexanone with hydrogen peroxide/benzonitrile over hydrotalcites as catalysts. *Appl. Catal. A Gen.* **2006**, *312*, 86–94. [[CrossRef](#)]
14. Ruiz, J.R.; Jimenez-Sanchidrian, C.; Llamas, R. Hydrotalcites as catalysts for the Baeyer-Villiger oxidation of cyclic ketones with hydrogen peroxide/benzonitrile. *Tetrahedron* **2006**, *62*, 11697–11703. [[CrossRef](#)]
15. Llamas, R.; Jiménez-Sanchidrián, C.; Ruiz, J.R. Heterogeneous Baeyer-Villiger oxidation of ketones with H₂O₂/nitrile, using Mg/Al hydrotalcite as catalyst. *Tetrahedron* **2007**, *63*, 1435–1439. [[CrossRef](#)]
16. Llamas, R.; Jiménez-Sanchidrián, C.; Ruiz, J.R. Metal hydroxides as catalysts for the Baeyer-Villiger oxidation of cyclohexanone with hydrogen peroxide. *React. Kinet. Catal. Lett.* **2007**, *90*, 309–313. [[CrossRef](#)]
17. Llamas, R.; Jiménez-Sanchidrián, C.; Ruiz, J.R. Environmentally friendly Baeyer-Villiger oxidation with H₂O₂/nitrile over Mg(OH)₂ and MgO. *Appl. Catal. B Environ.* **2007**, *72*, 18–25. [[CrossRef](#)]
18. Cavani, F.; Trifiro, F.; Vaccari, A. Hydrotalcite-type anionic clays: Preparation, properties and applications. *Catal. Today* **1991**, *11*, 173–301. [[CrossRef](#)]
19. Nalawade, P.; Aware, B.; Kadam, V.J.; Hirlekar, R.S. Layered double hydroxides: A review. *J. Sci. Ind. Res.* **2009**, *68*, 267–272.
20. Wang, Q.; O'Hare, D. Recent advances in the synthesis and application of layered double hydroxide (LDH) nanosheets. *Chem. Rev.* **2012**, *112*, 4124–4155. [[CrossRef](#)]
21. Kaneda, K.; Mizugaki, T. Design of high-performance heterogeneous catalysts using hydrotalcite for selective organic transformations. *Green Chem.* **2019**, *21*, 1361–1389. [[CrossRef](#)]
22. Saifullah, B.; Hussein, M.Z.B. Inorganic nanolayers: Structure, preparation, and biomedical applications. *Int. J. Nanomed.* **2015**, *10*, 5609.
23. Rives, V.; Arco, M.D.; Martín, C. Intercalation of drugs in layered double hydroxides and their controlled release: A review. *Appl. Clay Sci.* **2014**, *88*, 239–269. [[CrossRef](#)]
24. Yue, X.; Li, C.; Ni, Y.; Xu, Y.; Wang, J. Flame retardant nanocomposites based on 2D layered nanomaterials: A review. *J. Mater. Sci.* **2019**, *54*, 13070–13105. [[CrossRef](#)]
25. Hoxha, A.; Gillam, D.G.; Bushby, A.J.; Agha, A.; Patel, M.P. Layered double hydroxide fluoride release in dental applications: A systematic review. *Dent. J.* **2019**, *7*, 87. [[CrossRef](#)] [[PubMed](#)]
26. Roth, W.J.; Gil, B.; Makowski, W.; Marszalek, B.; Eliášová, P. Layer like porous materials with hierarchical structure. *Chem. Soc. Rev.* **2016**, *45*, 3400–3438. [[CrossRef](#)] [[PubMed](#)]
27. Prevot, V.; Tokudome, Y. 3D hierarchical and porous layered double hydroxide structures: An overview of synthesis methods and applications. *J. Mater. Sci.* **2017**, *52*, 11229–11250. [[CrossRef](#)]
28. Xie, W.; Li, Z.; Shao, M.; Wei, M. Layered double hydroxide-based core-shell nanoarrays for efficient electrochemical water splitting. *Front. Chem. Sci. Eng.* **2018**, *12*, 537–554. [[CrossRef](#)]
29. Jiang, S.D.; Song, L.; Zeng, W.R.; Huang, Z.Q.; Zhan, J.; Stec, A.A.; Hull, T.R.; Hu, Y.; Hu, W.Z. Self-assembly fabrication of hollow mesoporous Silica@Co-Al Layered Double Hydroxide@Graphene and application in toxic effluents elimination. *ACS Appl. Mater. Interfaces* **2015**, *7*, 8506–8514. [[CrossRef](#)]
30. Shirotori, M.; Nishimura, S.; Ebitani, K. Effect of SiO₂ amount on heterogeneous base catalysis of SiO₂@Mg-Al layered double hydroxide. *RSC Adv.* **2018**, *8*, 28024–28031. [[CrossRef](#)]
31. Jiang, S.D.; Bai, Z.M.; Tang, G.; Song, L.; Stec, A.A.; Hull, T.R.; Hu, Y.; Hu, W.Z. Synthesis of mesoporous silica@Co-Al layered double hydroxide spheres: Layer-by-layer method and their effects on the flame retardancy of epoxy resins. *ACS Appl. Mater. Interfaces* **2014**, *6*, 14076–14086. [[CrossRef](#)]
32. Yilmaz, M.S. Synthesis of novel amine modified hollow mesoporous silica@Mg-Al layered double hydroxide composite and its application in CO₂ adsorption. *Microporous Mesoporous Mater.* **2017**, *245*, 109–117. [[CrossRef](#)]
33. Zou, H.; Wu, S.; Shen, J. Polymer/Silica Nanocomposites: Preparation, Characterization, Properties, and Applications. *Chem. Rev.* **2008**, *108*, 3893–3957. [[CrossRef](#)]
34. Soler-Illia, G.J.D.A.A.; Sanchez, C.; Lebeau, B.; Patarin, J. Chemical strategies to design textured materials: From microporous and mesoporous oxides to nanonetworks and hierarchical structures. *Chem. Rev.* **2002**, *102*, 4093–4138. [[CrossRef](#)]
35. Jankiewicz, B.J.; Jamiola, D.; Choma, J.; Jaroniec, M. Silica—Metal core—Shell nanostructures. *Adv. Colloid Interface Sci.* **2012**, *170*, 28–47. [[CrossRef](#)]
36. Chen, C.; Wang, P.; Lim, T.T.; Liu, L.; Liu, S.; Xu, R. A facile synthesis of monodispersed hierarchical layered double hydroxide on silica spheres for efficient removal of pharmaceuticals from water. *J. Mater. Chem. A* **2013**, *1*, 3877–3880. [[CrossRef](#)]

37. Cosano, D.; Esquivel, D.; Puertas, A.J.; Romero-Salguero, F.J. Microstructural analysis of 3D hierarchical composites of hydrotalcite-coated silica microspheres. *Microporous Mesoporous Mater.* **2021**, *323*, 111247. [CrossRef]
38. Aramendía, M.A.; Borau, V.; Jiménez, C.; Marinas, J.M.; Ruiz, J.R.; Urbano, F.J. Catalytic hydrogen transfer from 2-propanol to cyclohexanone over basic Mg–Al oxides. *Appl. Catal. A Gen.* **2003**, *255*, 301–308. [CrossRef]
39. Thommes, M.; Kaneko, K.; Neimark, A.V.; Olivier, J.P.; Rodriguez-Reinoso, F.; Rouquerol, J.; Sing, K.S.W. Physisorption of gases, with special reference to the evaluation of surface area and pore size distribution (IUPAC Technical Report). *Pure Appl. Chem.* **2015**, *87*, 1051–1069. [CrossRef]
40. Olszówka, J.; Karcz, R.; Napruszewska, B.; Bielańska, E.; Dula, R.; Krzan, M.; Nattich-Rak, M.; Socha, R.P.; Klimek, A.; Bahranowski, K.; et al. Magnesium and/or calcium-containing natural minerals as ecologically friendly catalysts for the Baeyer–Villiger oxidation of cyclohexanone with hydrogen peroxide. *Appl. Catal. A Gen.* **2016**, *509*, 52–65. [CrossRef]
41. Karcz, R.; Napruszewska, B.D.; Michalik, A.; Kryściak-Czerwenka, J.; Duraczyńska, D.; Serwicka, E.M. Fine crystalline Mg–Al hydrotalcites as catalysts for baeyer-villiger oxidation of cyclohexanone with H₂O₂. *Catalysts* **2021**, *11*, 1493. [CrossRef]
42. Li, J.; Le, Y.; Dai, W.L.; Li, H.; Fan, K. Self-assembled Mg₅(CO₃)₄(OH)₂·4H₂O nanosheet as an effective catalyst in the Baeyer–Villiger oxidation of cyclohexanone. *Catal. Commun.* **2008**, *9*, 1334–1341. [CrossRef]
43. Paul, M.; Pal, N.; Mondal, J.; Sasidharan, M.; Bhaumik, A. New mesoporous magnesium-aluminum mixed oxide and its catalytic activity in liquid phase Baeyer–Villiger oxidation reaction. *Chem. Eng. Sci.* **2012**, *71*, 564–572. [CrossRef]
44. Stöber, W.; Fink, A. Controlled Growth of Monodisperse Silica Spheres in the Micron Size Range. *J. Phys. Ther. Sci.* **1968**, *26*, 62–69. [CrossRef]
45. JCPDS Joint Committee on Powder Diffraction Standards (Now: International Centre for Diffraction Data). 1991. Available online: www.icdd.com (accessed on 15 May 2022).
46. Reichle, W.T.; Kang, S.Y.; Everhardt, D.S. The nature of the thermal decomposition of a catalytically active anionic clay mineral. *J. Catal.* **1986**, *101*, 352–359. [CrossRef]
47. Taniya, K.; Mori, R.; Okemoto, A.; Horie, T.; Ichihashi, Y.; Nishiyama, S. Role of Al³⁺ species in beta zeolites for Baeyer–Villiger oxidation of cyclic ketones by using H₂O₂ as an environmentally friendly oxidant. *Catal. Today* **2018**, *307*, 293–300. [CrossRef]
48. Alegria, E.C.B.A.; Martins, L.M.D.R.S.; Kirillova, M.V.; Pombeiro, A.J.L. Baeyer–Villiger oxidation of ketones catalysed by rhenium complexes bearing N- or oxo-ligands. *Appl. Catal. A Gen.* **2012**, *443–444*, 27–32. [CrossRef]
49. Meng, Q.; Liu, J.; Xiong, G.; Liu, X.; Liu, L.; Guo, H. Aerosol-seed-assisted hydrothermal synthesis of Sn-Beta zeolite and its catalytic performance in Baeyer–Villiger oxidation. *Microporous Mesoporous Mater.* **2018**, *266*, 242–251. [CrossRef]
50. Olszówka, J.E.; Karcz, R.; Michalik-Zym, A.; Napruszewska, B.D.; Bielańska, E.; Kryściak-Czerwenka, J.; Socha, R.P.; Nattich-Rak, M.; Krzan, M.; Klimek, A.; et al. Effect of grinding on the physico-chemical properties of Mg–Al hydrotalcite and its performance as a catalyst for Baeyer–Villiger oxidation of cyclohexanone. *Catal. Today* **2019**, *333*, 147–153. [CrossRef]
51. Han, Y.; Li, S.; Ding, R.; Xu, W.; Zhang, G. Baeyer–Villiger oxidation of cyclohexanone catalyzed by cordierite honeycomb washcoated with Mg–Sn–W composite oxides. *Chinese J. Chem. Eng.* **2019**, *27*, 564–574. [CrossRef]
52. Olszówka, J.E.; Karcz, R.; Napruszewska, B.D.; Michalik-Zym, A.; Duraczyńska, D.; Kryściak-Czerwenka, J.; Niecikowska, A.; Bahranowski, K.; Serwicka, E.M. Effect of Mg–Al hydrotalcite crystallinity on catalytic Baeyer–Villiger oxidation of cyclohexanone with H₂O₂/acetonitrile. *Catal. Commun.* **2018**, *107*, 48–52. [CrossRef]